



HAL
open science

Microwave assisted freezing part 1: Experimental investigation and numerical modeling

Mathieu Sadot, Sébastien Curet, Alain Le-Bail, Olivier Rouaud, Michel Havet

► **To cite this version:**

Mathieu Sadot, Sébastien Curet, Alain Le-Bail, Olivier Rouaud, Michel Havet. Microwave assisted freezing part 1: Experimental investigation and numerical modeling. *Innovative Food Science & Emerging Technologies / Innovative Food Science and Emerging Technologies*, 2020, 62, pp.102360. 10.1016/j.ifset.2020.102360 . hal-02611589

HAL Id: hal-02611589

<https://hal.science/hal-02611589v1>

Submitted on 22 Aug 2022

HAL is a multi-disciplinary open access archive for the deposit and dissemination of scientific research documents, whether they are published or not. The documents may come from teaching and research institutions in France or abroad, or from public or private research centers.

L'archive ouverte pluridisciplinaire **HAL**, est destinée au dépôt et à la diffusion de documents scientifiques de niveau recherche, publiés ou non, émanant des établissements d'enseignement et de recherche français ou étrangers, des laboratoires publics ou privés.



HAL Authorization

Microwave assisted freezing

Part 1: Experimental investigation and numerical modeling

**Mathieu SADOT, Sébastien CURET, Alain LE-BAIL, Olivier ROUAUD,
Michel HAVET**

Abstract

The aim of this study was to develop an innovative process dedicated to enhancing the quality of frozen food using microwaves. A microwave assisted freezing device was designed at the laboratory scale to perform experiments in controlled conditions. Small samples of methylcellulose gels were frozen using nitrogen gas in a TE₁₀ waveguide, where microwaves at 2.45 GHz were emitted intermittently or continuously. A numerical model was also developed to obtain results difficult to measure such as the local electric field and the corresponding energy density. The phase change part of the model was based on an enthalpy formulation and on the growth of spherical ice crystals. An original “hybrid 2D-3D” solving methodology was used to reduce the duration of the simulations. Favourable comparisons between the predicted temperatures and the experimental data highlighted the relevance of the models used for the thermophysical and dielectric properties. The analysis of the interactions between microwaves and matter, performed with numerical simulations, revealed the role of the freezing front as a boundary. The strong influence of sample size and of dielectric properties on the power density distribution were also illustrated when comparing our results with those published previously. The scientific knowledge obtained through this study and the original structure of the numerical model will be used to optimize microwave assisted freezing and link the process parameters to the reduction of ice crystal size highlighted in the companion paper.

Keywords

Freezing; microwaves; modelling; ice fraction;

Highlights

- A device was built to perform microwave assisted freezing in a controlled configuration.
- A hybrid 2D-3D model was developed to decrease computation time.
- The numerical model was validated against experimental results.
- All food properties were modelled using the ice fraction during freezing.
- The interactions between the EM field and the freezing front were highlighted by the simulations.

34

35 Industrial relevance

36 Microwave assistance during freezing can improve frozen product quality by reducing ice crystal size.
37 This innovative and promising process has not yet been given much attention. Developing an
38 accurate model which describes microwave – matter interactions during phase change permits
39 numerical simulations that can facilitate the design of industrial equipment, and determine optimal
40 product dimensions.

41

42 1. Introduction

43 Freezing is one of the most widely used conservation processes in the food industry; low storage
44 temperatures allow good preservation of product organoleptic (texture, taste, appearance) and
45 nutritive (vitamins, minerals) qualities. It reduces chemical reaction rates (Lim et al., 2004) and
46 controls microbial activity (Bremer & Ridley, 2004).

47 The quality of a frozen product is generally better when smaller ice crystals are formed (Delgado &
48 Sun, 2001) because larger ones damage cell membranes due to water expansion during the phase
49 change (Kalichevsky et al., 1995). These small crystals are usually obtained for faster freezing
50 processes (Devine et al., 1996) but fast freezing processes (e.g. cryogenics) are known to be energy-
51 demanding (Chourot et al., 2003; Dempsey & Bansal, 2012).

52 In recent years, growing interest in innovative freezing processes has led to increased frozen product
53 quality while reducing ice crystal size, using ultrasound, magnetic fields, AC and DC electric fields,
54 mechanical agitation, and pressure shift freezing (Dalvi-Isfahan et al., 2017; Jha et al., 2017; Le Bail et
55 al., 2002; Woo & Mujumdar, 2010). Electromagnetic wave assisted freezing is one of the less
56 investigated processes although some studies have presented interesting results. Apart from the
57 simple main principle that consists in applying an electromagnetic field during the freezing process, it
58 entails several modalities and configurations. It was first studied by Hanyu et al. (1992) and Jackson
59 et al.(1997) who used 2450 MHz microwave irradiation on non-food material during freezing. Hanyu
60 et al.(1992) found a reduction in ice crystal size in squid retina that resulted in better ultrastructural
61 preservation. Jackson et al. (1997) obtained less ice and more glass in an aqueous ethylene glycol
62 solution. More recent works have focused on electromagnetic wave assistance during food freezing.
63 Anese et al. (2012) and Hafezparast-moadab et al. (2018) used 27.12 MHz radiofrequency (RF) wave
64 irradiation during freezing. Anese et al. (2012) froze pork with liquid nitrogen and obtained better
65 product quality when the product was frozen under electromagnetic wave irradiation. The crystals
66 were also found to be smaller with the use of RF assistance. Hafezparast-moadab et al. (2018) froze

67 trout with a cold air convection system with and without RF assistance. They observed a reduction in
68 ice crystal size up to 75% in the better case in comparison to conventional freezing. Microwave
69 assisted freezing at 2450 MHz was investigated by Xanthakis et al. (2014). They also showed a
70 reduction in ice crystal size when microwave assistance was used.

71 Despite these promising results, there is a lack of information on the physical mechanisms involved in
72 the improvement of the freezing process by microwaves. The European FREEZEWAVE project (FP7-
73 ERA-Net SUSFOOD) was initiated to help understanding these phenomena. The project goals were to
74 develop and optimize a lab scale batch process and to develop a new model in order to improve
75 scientific knowledge on microwave assisted process. This project also aimed to assess the effect of
76 microwaves on reduction of the ice crystal size to improve frozen foods quality and scale up to
77 industrial scale for batch and continuous processes.

78 Most of the experiments anterior to FREEZEWAVE project were performed in multi-mode cavities
79 where microwave distribution is heterogeneous and cannot be determined; especially in the case of
80 pulsed or intermittent waves. In the duty cycles applied temperature fluctuations were considered to
81 be at the origin of promising results, but interactions between the matrices and the microwaves
82 could not be analysed in-depth. The only numerical study on the interaction of microwaves and
83 matter during freezing was performed previously in the FREEZEWAVE project to help obtain better
84 understanding of these phenomena (Sadot et al., 2017). The resonance phenomena inside the
85 product were identified and revealed the displacement of hot spots during the phase change,
86 induced by the decrease in dielectric properties with temperature. Nevertheless, this pioneering
87 work was based on a model that was not validated against the experimental data of a microwave
88 assisted freezing process. Moreover, the physical and electrical properties were taken from the
89 literature.

90 Taking into account these considerations, the aim of the current study is to: (i) design an
91 experimental device to conduct microwave assisted freezing experiments in controlled conditions
92 with temperature measurements inside the matrices; (ii) conduct experiments on a small sample in
93 which the treatment is expected to be homogeneous; (iii) define and use protocols in order to
94 measure the properties required as inputs in the model; and (iv) validate the model against real
95 experimental data.

96 2. Materials and methods

97 2.1. Product

98 For this study, experiments had to be conducted on a homogeneous product, which can be made
99 with good repeatability, in order to conserve the same properties. This is why we chose
100 methylcellulose gel whose thermophysical and dielectric properties are close to those of food,

101 especially meat (Pangrle et al., 1992; Taoukis et al., 1987; Zhang & Datta, 2005). Methylcellulose gels
102 at 13% (w/w) were prepared by progressively adding 15 g of methylcellulose powder (Tylose H
103 100000 YP2, ShinEtsu, Jp) into 100 g of demineralized water agitated with a magnetic stirrer. The
104 solution was then poured into a Polyether ether ketone (PEEK) mould of 10 mm height, 39 mm
105 length and 9 mm width and hermetically stored at 4°C for at least 10 h. To avoid the development of
106 microorganisms and the occurrence of air bubbles, the gel was not stored for more than 4 days. The
107 PEEK moulds were inserted into polystyrene sample holders to ensure good insulation during the
108 freezing experiments.

109 2.2. Experimental device

110 An experimental device was developed (Figure 1) to study the microwave assisted freezing of this gel
111 in controlled conditions. In the FREEZEWAVE project, this device must also be able to treat real food
112 matrices.

113 Nitrogen is transferred from a compressed gas cylinder (1) into a liquid nitrogen tank (2), in which a
114 steel pipe is immersed. The liquid nitrogen is injected into the pipe where it vaporises and increases
115 in temperature. The end of the pipe is equipped with a heating part (3) used to control the
116 temperature at the inlet of the applicator (4) in which the product (5) is placed. The applicator is
117 located in a rectangular waveguide WR 340 (section 86 mm x 43 mm), to ensure the propagation of
118 the fundamental single-mode TE₁₀ at a frequency of 2450 MHz (electric field perpendicular to the
119 wave propagation direction with an extremum at the centre of the long walls, a zero value at the
120 small walls and a constant value along the small side). Two slits of 10 mm height, perpendicular to
121 the microwave propagation direction, were machined along the small walls of the applicator flange
122 to allow the inlet and the outlet of the nitrogen gas. The nitrogen gas is then extracted outside the
123 building in which the experiment takes place. Holes of 0.5 mm were drilled every 5 mm along the
124 centre of the small waveguide wall to insert sheathed thermocouples through the waveguide, the
125 polystyrene and the PEEK to the sample in order to measure temperature during microwave assisted
126 freezing. Thermocouples, electrically connected to the waveguide walls, are sheathed/isolated to
127 avoid electric arc formation.

128 Microwaves are continuously emitted by a solid-state generator (GMS200, SAIREM, France) (6). They
129 are transmitted to the waveguide via a switch (7). This permits the generation of pulses by sending
130 the microwaves alternatively to an adapted absorptive load (8) and to an antenna (9) located at the
131 inlet of the waveguide. After passing through the microwave applicator, the microwave power
132 transmitted is absorbed by a water-load (10) to avoid any reflection.

133 With this configuration, microwaves and nitrogen reach the product on the top surface. The
 134 microwaves are expected to pass through the frozen product with very little attenuation because of
 135 the low dielectric properties of the frozen product. Therefore, the microwaves can act on the phase
 136 change via the hot spots able to follow the freezing front (Sadot et al., 2017). Unlike this previous
 137 numerical study, the product does not fill the entire waveguide cross-section. The mould containing
 138 the sample is centred as shown in Figure 1 (11) and surrounded by polystyrene (except the cooled
 139 surface) to ensure thermal insulation. The sheathed thermocouples are inserted at depths of 2 mm
 140 and 7 mm (along the z axis), as shown in Figure 2.

141 3. Model

142 The model used in this study is based on an enthalpy formulation of the heat equation (Eq. 1) with a
 143 source term derived from Maxwell equation (Eq. 2).

$$\frac{\partial H}{\partial t} \rho - \nabla \cdot k \nabla T = Q \quad (1)$$

$$Q = \frac{1}{2} \omega \epsilon_0 \epsilon'' |E_{local}|^2 \quad (2)$$

144 This model was developed previously and is fully detailed in Sadot et al. (2017). The phase change
 145 model is based on the ice mass fraction that depends on crystal volume growth. The thermophysical
 146 and dielectric properties vary with the ice mass fraction as the water state is assumed to be the only
 147 parameter responsible for the variation of properties.

148 3.1. Hypotheses and boundary conditions

149 Several hypotheses are made to model the system:

150 _The product is assumed to be homogeneous.

151 _The mass transfer is neglected because of the small specific area and the speed of cryogenic
 152 freezing (Delgado & Sun, 2001; Hallstrom, 1990).

153 Heat transfer equations are solved only in the product sample with the following boundaries:

154 _The initial temperature is assumed constant within the product.

$$T = T_0 \quad \text{at } t = 0, \forall x, y, z \quad (3)$$

155 _The heat transfer between the product and the nitrogen is assumed to be homogeneous on the
 156 entire surface.

$$n(k \nabla T) = -h(T - T_{N_2}) \quad \text{at } z = 0 \text{ (top surface), } \forall x, y \quad (4)$$

157 _The lateral walls of the product exchange heat with a global transfer loss coefficient:

$$n(k\nabla T) = -h_{\text{loss}}(T - T_{\text{air}}) \quad \text{at } x = -l/2 \text{ and } x = l/2 \text{ (surface), } \forall y, z \quad (5)$$

158 _The product bottom and the surfaces along the large waveguide walls are assumed to be thermally
159 insulated.

$$n(k\nabla T) = 0 \quad \text{at } z = -d, \forall x, y \quad (6)$$

$$n(k\nabla T) = 0 \quad \text{at } y = -L/2 \forall x, z \quad (7)$$

$$n(k\nabla T) = 0 \quad \text{at } y = L/2 \forall x, z \quad (8)$$

160 _The incident microwaves are generated on the inlet port in fundamental single-mode TE₁₀.

161 _The microwave power is absorbed without reflection at the waveguide outlet.

162 _The waveguide walls are assumed to be perfect electric conductors. There is therefore no
163 electromagnetic power loss at the waveguide walls.

$$n \times E = 0 \quad \text{at } x = -a/2 \text{ and } x = a/2, \forall y, z \quad (9)$$

$$n \times E = 0 \quad \text{at } y = -b/2 \text{ and } y = b/2, \forall x, z \quad (10)$$

164 3.2. Simulation settings

165 The simulations were performed with the finite element software COMSOL Multiphysics, on a
166 workstation with 256 GB RAM and an Intel® Xeon® CPU E5-2680 v3 processor, 12 cores, 2.50 GHz.
167 The mesh of the entire geometry, on which the electromagnetism is solved, is composed of 17672
168 tetrahedra measuring no more than 6.88 mm. The heat equation is solved in a sub-geometry with a
169 more refined mesh of 1318 tetrahedra, measuring no more than 1.00 mm. When solving both the
170 electromagnetism and the heat equation, a previous study showed that mesh independency is
171 obtained for a maximum element size of 1.75 mm (Sadot et al., 2017).

172 3.3. Input parameters for the model

173 The model required product properties (physical, thermal and electrical ones) and process
174 parameters like convective coefficient, nitrogen temperature and incident microwave power.

175 3.3.1. Physical and thermal properties

176 The dry matter of the product is measured by weighing gel samples before and after heating for 48 h
177 in a stove at 104°C. The gel density was measured at 20°C in a helium pycnometer Accupyc 1330
178 (Micromeritics, France). The measurement takes about 10 min, which makes it impossible in frozen
179 phase. Therefore, density in frozen phase is determined by a mixing model:

$$\rho_f = \left(\frac{x_i}{\rho_i} + \frac{x_{bw}}{\rho_w} + \frac{x_{dm}}{\rho_{dm}} \right)^{-1} \quad (11)$$

180 Methylcellulose powder density is also measured in the helium pycnometer.

181 The initial freezing temperature is a key parameter. During a slow freezing experiment in a domestic
182 apparatus, the evolution of the temperature was measured with thermocouples. The gel was not a

183 pure product, so the beginning of the pseudo plateau is assumed to be the initial freezing
184 temperature.

185 The thermal conductivity was obtained with the hot-wire probe method (Healy et al., 1976) at 5°C, -
186 15°C, -20°C and -25°C with a raise of 5°C. Because of the phase change, the thermal conductivity was
187 not measured at temperatures close to the initial freezing temperature because latent heat would
188 have caused a measurement error. In fresh state the thermal conductivity is assumed constant and
189 equal to the value measured at 5°C. The freezable water content and the heat capacity were
190 determined by differential scanning calorimetry on a μ DSC VII (TA Instrument, USA). Samples of 130
191 mg were introduced in a Hastelloy C alloy cell. The heat flux was measured for freezing from 20°C to -
192 40°C and for thawing from -40°C to 20°C at a rate of 1°C.min⁻¹ for two different samples. Because
193 water is the only component assumed to solidify, the freezable water content was determined by
194 calculating the ratio between the total enthalpy of the product and the latent heat of pure water.

195 3.3.2. Dielectric properties

196 The dielectric constant and dielectric loss factor were measured with an open-ended coaxial probe
197 (Dielectric Probe Kit 85070^E, high temperature configuration, Agilent Technologies) connected to an
198 electronic calibration module (85092-60010, Agilent Technologies). The probe was located in a
199 freezing cabinet (range 150, FROILABO, France). A low power microwave at the desired frequency
200 (2450 MHz) was emitted by a network analyser (E5062A, Agilent Technologies) to the surface of the
201 product (cylinder of 60 mm height and 35 mm diameter). The reflected microwaves from the product
202 surface were analysed by the network analyser that allowed determining the dielectric properties
203 using an algorithm. This method is well adapted to the food product dielectric properties
204 measurement (Sheen & Woodhead, 1999) and was recently used with success (Llave et al., 2016).
205 The measurements were performed at stabilised temperature between 20°C and -40°C.

206 3.3.3. Heat transfer coefficient

207 The lumped-capacitance method was used to measure the heat transfer coefficient between the
208 nitrogen and the gel surface. An aluminium bloc with the same dimensions as those of the sample,
209 with the same exposed surface and the same thermal insulation, was used. Aluminium was chosen
210 because of its high thermal conductivity, which enables assuming a homogeneous temperature
211 within this small volume. Assuming the perfect insulation of the aluminium bloc by the polystyrene
212 on the surfaces not exposed to the nitrogen, the following equation can be written:

$$mCp \frac{dT_{alu}}{dt} = hS(T_{N_2} - T_{alu}) \quad (12)$$

213 The nitrogen gas temperature has to be as constant as possible. The nitrogen delivery pipe is cooled,
214 and then connected to the applicator once the temperature is stable. The convection coefficient is
215 obtained by plotting:

$$\frac{mC_p}{S} \ln \frac{T_0 - T_{N_2}}{T_{atu} - T_{N_2}} = f(t) \quad (13)$$

216 The straight-line slope obtained provides the convection coefficient.

217 3.3.4. Incident microwave Power

218 A power measurement system is included in the microwave generator. Nevertheless, because of
219 possible power losses (in connectors, coaxial cables, waveguide walls, etc.) between the emitter and
220 the applicator, a power calibration was performed on microwave heating in simple conditions.

221 4. Results and discussion

222 4.1. Methylcellulose gel properties

223 4.1.1. Density

224 To validate the mixing model of density in the frozen phase, it was first used to calculate the
225 methylcellulose gel density from water and methylcellulose powder densities in fresh state. The
226 calculated density and the measured density at 18°C were 1040.5 kg.m⁻³ and 1065 ± 15.47 kg.m⁻³
227 respectively. The relative difference of 2.33% was low enough to allow the use of the mixing model in
228 the frozen phase. The density of the frozen gel obtained from the methylcellulose powder and ice
229 densities was 966 kg.m⁻³. Although there was a little difference between the frozen and fresh gel
230 densities, the volume variation during the process (7.5%) was neglected. The frozen and fresh gel
231 densities were used only to solve the heat equation.

232 4.1.2. Dry matter content

233 The dry matter measured was 0.129kg.kg⁻¹_{product} ± 0.001 kg.kg⁻¹_{product}, which is logical regarding the
234 formulation of the gel (13% powder).

235 4.1.3. Initial freezing temperature

236 Because of its considerable hydration, the beginning of the methylcellulose gel freezing plateau was
237 horizontal. The initial freezing temperature was determined graphically at -0.7°C from the plateau
238 following the supercooling break.

239 4.1.4. Thermal conductivity

240 The methylcellulose gel thermal conductivities measured from the hot-wire probe method are
241 shown in Table 1. The values are in the range of data measured by previous authors (Otero et al.,
242 2006; Singh & Heldman, 2014).

243 4.1.5. Freezable and bound water content

244 The latent heats obtained by DSC for freezing and thawing are presented in Table 2.

$$x_{fw} = \frac{Hf_{gel}}{Hf_w} = \frac{253.23}{332} = 0.7627 \text{ kg}_w \cdot \text{kg}_{product}^{-1} \quad (14)$$

$$x_{bw} = x_w - x_{fw} = 0.8709 - 0.7627 = 0.1082 \text{ kg}_w \cdot \text{kg}_{product}^{-1} \quad (15)$$

245 The freezable water content is $0.7627 \text{ kg} \cdot \text{kg}^{-1}$ of product and the bound water content is
246 $0.1082 \text{ kg} \cdot \text{kg}^{-1}$ of product.

247 4.1.6. Heat capacity

248 The heat capacity measured in fresh (20°C) and frozen (-20°C) phase is shown in Table 3.

249 4.1.7. Dielectric properties

250 The dielectric properties are presented in Figure 3. To the best of our knowledge, the dielectric
251 properties of methylcellulose gel with 87% water content had not yet been measured
252 experimentally. Nevertheless, during thawing, the evolution of dielectric properties as a function of
253 temperature was very similar to that of other studies although the order of magnitude changed
254 slightly due to a difference in hydration level (Llave et al., 2016) or due to the addition of salt (Nelson
255 & Datta, 2001). The temperature dependencies of ϵ' and ϵ'' were observed in fresh state, especially
256 for the dielectric loss factor (60% from 40°C to 0°C). Once the temperature reached the initial
257 freezing point, an abrupt decrease in dielectric properties could be seen. Then, as the temperature
258 decreased, the dielectric properties tended to stabilise around -10°C . This decrease of the dielectric
259 loss factor as a function of temperature is commonly observed for a methylcellulose gel in fresh state
260 without any addition of salt (Llave et al., 2016). With the gel used in the current study, the dielectric
261 loss factor was more than 100 times lower at -20°C (0.25) than at 0°C (29).

262 As dielectric properties do not change greatly in the frozen phase, they were therefore considered
263 constant in the model. The evolution of dielectric properties in the frozen phase was thus a function
264 of the mixing model which depended on the ice fraction (Sadot et al., 2017). However, as they vary
265 too much in fresh state, their variation was taken into account.

266 4.2. Convection coefficient

267 The convection coefficients between nitrogen and the aluminium bloc measured experimentally are
268 reported in Table 4 for different trials.

269 Large differences in convection coefficient values were found. The measurement was reproducible
270 but the nitrogen flowrate varied. The experimental device was equipped with a safety valve, which
271 opened to avoid overpressure and induced nitrogen flow variations. Because of these variations, the
272 convection coefficient was used as a fitting parameter in the range of the values measured.

273 4.3. Calibration of incident microwave power

274 The incident power at the applicator inlet had to be calibrated because of possible losses between
275 the microwave generator and the applicator. 3D numerical simulations were performed on specific
276 experiments of microwave heating of samples at ambient temperature for 1 minute. As the incident
277 power was the only unknown parameter, it was calibrated by fitting the experimental temperature
278 data with a numerical prediction.

279 As expected, the power supplied by the generator was higher than the incident power at the
280 applicator inlet used as a boundary condition in the simulations. The generator power had to be
281 corrected by a factor equal to 0.75 to obtain the incident power at the applicator inlet. This value
282 was in the range of the typical efficiency factor, which varies between 0.5 and 0.9 (Cherbanski,
283 2011; Wang et al., 2015). In these conditions, the resulting simulated temperature curves are very
284 close to the experimental ones (Figure 4). The slight difference observed, approximately 1°C, can be
285 attributed to the hypothesis made for the simulation (such as perfect thermal insulation), and to
286 experimental uncertainties. The calibration factors obtained from these heating experiments were
287 applied for all the further microwave assisted freezing experiments.

288 4.4. Development of the hybrid 2D-3D model

289 The computation time of microwave assisted freezing can be very long. As a 4 g sample can be frozen
290 in less than an hour experimentally, the computation can last more than a week. Thus a hybrid model
291 was developed to reduce the computation time. The resolution of the electric field induced a 3D
292 simulation because the geometry used in this study did not allow any geometrical simplifications
293 along the y-axis (Figure 2). However, the heat equation did not need to be solved in 3D because the
294 heat transfer was assumed to be homogeneous along the y-axis (Figure 2). The heat equation was
295 then solved in 3D for a thin layer of 1 mm along the y axis, as shown in Figure 2b. This simplification
296 can be assimilated to a 2D resolution on the x-z plan at $y = 0$. The temperature and thus the

297 temperature dependant dielectric properties required to solve Maxwell's equations are considered
298 constant along the y axis.
299 The results of hybrid and 3D models were compared for the microwave heating trial used to calibrate
300 the incident power at the applicator inlet (Figure 5). As the temperature curves at 2 mm and 7 mm
301 depth are very similar, it allows concluding that the hybrid model is relevant with this geometry.
302 Moreover, in this simple case of microwave heating without phase change, the hybrid model was 19
303 times faster than the full 3D model (3 min 48 s vs 71 min).

304 4.5. Model validation

305 The current model was assessed previously (Sadot et al., 2017) in comparison to cryogenic freezing
306 (Rouaud & Le-bail, 2015) and microwave heating (Curet, 2008) because previous experimental
307 studies did not provide any exploitable data of microwave assisted freezing. According to our
308 knowledge, the current study is the first to provide relevant data available for model validation. In
309 the current study, the results of the model are compared to experimental results in controlled
310 conditions for the same geometry as that used for the microwave heating (Figure 2).

311 The global thermal losses at the product lateral walls were found to be low. The global thermal loss
312 coefficient ranged between $4.5 \text{ W}\cdot\text{m}^{-2}\cdot\text{K}^{-1}$ and $5 \text{ W}\cdot\text{m}^{-2}\cdot\text{K}^{-1}$. For all the simulations, the empirical
313 parameter of crystal growth (Y in Eq 6) was set to 0.75 K and provided the following ice content in
314 the gel (Figure 6). The ice mass fraction is dependent on the freezing kinetics. The empirical
315 parameter could not be determined by DSC by adjusting the freezing rate because of the
316 supercooling phenomenon that occurs systematically during freezing in the DSC oven.

317 Validation was done first for continuous applied microwave assisted freezing at a power of 1 W. The
318 convection coefficient was set at $95 \text{ W}\cdot\text{m}^{-2}\cdot\text{K}^{-1}$ on the cooled surface (Figure 7a). The model was then
319 used for pulsed microwave assisted freezing for a duty ratio of 0.33 and a power of 3 W (Figure 7b),
320 as electromagnetic wave assisted freezing was mainly performed with pulses in the literature (Anese
321 et al., 2012; Hafezparast-moadab et al., 2018; Xanthakis et al., 2014). In this second case, the
322 convection coefficient was $87.5 \text{ W}\cdot\text{m}^{-2}\cdot\text{K}^{-1}$.

323 In both cases, there was very good agreement between the simulated and experimental temperature
324 curves, although the temperature at 2 mm depth was slightly underestimated by the model. For
325 pulsed microwave assisted freezing, the temperature oscillations were about 1°C at 7 mm depth in
326 both the simulation and the experiment. At 2 mm depth, the temperature oscillations were smaller
327 in the simulation due to small uncertainties. It is also noteworthy that the temperature oscillations
328 disappeared once the initial freezing was reached and thus when the dielectric properties started to
329 decrease. The good agreement between the simulations and the experiments validated the model,

330 thereby making it possible to obtain information on phenomena previously impossible to obtain
331 experimentally, such as electric field and generated heat distribution.

332 4.6. Analysis of interactions between microwaves and matter

333 The numerical study of microwave assisted freezing was conducted on continuous applied
334 microwave assisted freezing at a power of 1 W. The electric field and the generated heat are plotted
335 on the x-z central product section ($y = 0$) at several times (Figure 8).

336 First, we note that, contrary to the study in which the entire section (86×43 mm) was filled to a
337 height exceeding 30 mm (Sadot et al., 2017), the heterogeneity of the electric field distribution was
338 narrower (on the top surface the relative difference between the centre and the edges was 25% vs
339 95% in fresh state whereas it was 1% vs 95% in frozen state). This means that the objective of this
340 geometry, i.e. to obtain considerable homogeneity in treatment along x axis (Figure 2), was achieved.

341 Secondly, the product was smaller in height (z axis) than in the previous study (Sadot et al., 2017).
342 Only one maximum electric field appears in both the fresh and frozen phases (Figure 8a, c). After 15
343 minutes of microwave assisted freezing, two extrema of local electric field were visible due to the
344 two phases separated by the freezing front (Figure 8b). There was only one local maximum of
345 generated heat (hot spot), whose location corresponded to the local maximum of electric field in the
346 fresh state (Figure 8d, e, f). After 15 min of freezing, although the electric field distribution was
347 heterogeneous, it was in the same order of magnitude in the two phases (Figure 8b, Figure 9). The
348 generated heat distribution was much more heterogeneous. It was much lower in the frozen phase
349 compared to the fresh phase (Figure 8e, Figure 10). The freezing front, defined as the location where
350 the temperature is at the initial freezing point, marks a clear separation of heat generated due to the
351 reduction in dielectric loss factor, which was more than 100 times lower in frozen state (0.25 at -
352 20°C) than in fresh state (29 at 0°C). Once the phase change began, the generated heat became very
353 low (Figure 10) due to the fast decrease in dielectric loss factor (Figure 3).

354 In the previous numerical study (Sadot et al., 2017), the heat generated was high in the frozen phase
355 because of the high electric field value and of the dielectric loss factor value taken from the literature
356 (1.5 (Basak & Ayappa, 1997)) which was 6 times higher than the value measured in the current study
357 (0.25).

358 The interest of using the numerical simulation of microwave assisted freezing results in better
359 understanding of the interactions between microwaves and products during freezing. The
360 significance of product height regarding homogeneous microwave treatment was presented here as
361 an example in comparison with our previous study. It will be important to design the sample
362 dimensions to study the impact of microwaves during freezing on ice crystal size. However, it is still

363 complicated to determine certain model inputs such as incident microwave power at the applicator
364 inlet due to power losses.

365 5. Conclusion

366 A laboratory scale microwave assisted freezing process was designed to conduct experiments with
367 parameters and conditions that were controlled as much as possible. The thermophysical and
368 dielectric properties of the methylcellulose gel were accurately measured and the incident power
369 was determined by the inverse method. A numerical model, developed previously, was improved by
370 using a hybrid method to solve the heat equation in 2D and the Maxwell equations in 3D. The
371 significant reduction of computational time allowed the validation of the model in comparison to the
372 experimental data with this geometry.

373 The results showed that the ice mass fraction approach that we proposed is relevant for describing
374 all the evolutions of all the thermophysical and dielectric properties during phase change. The ice
375 mass fraction can also be used to define the enthalpy variation in the range of temperature studied.

376 The numerical simulations used to observe the evolution of the temperature within the product were
377 in very good agreement with the experiments. They pointed out temperature oscillations only in the
378 fresh state before the phase change, when microwaves were applied by pulses. We also observed
379 the electric field and heat distribution generated in a small sample. Only one hot spot was detected
380 in both the entire fresh and the entire frozen sample (Figure 8d, e, f, Figure 10). During freezing, one
381 maximum electric field was found in each phase, separated by the freezing front. In the frozen phase,
382 the heat generated was much lower than in the fresh phase because of the huge decrease in
383 dielectric loss factor during freezing.

384 The present study first confirmed that this new experimental device is relevant for conducting
385 microwave assisted freezing experiments in controlled conditions. It also emphasised the importance
386 of product dimensions, especially height and width, for the thermal homogeneity of the product
387 during this novel freezing process. The results from this numerical simulation are very useful for
388 determining the optimal dimension of a sample that could be used to analyse the impact of
389 microwave treatment on ice crystal size. This is the main objective of the companion paper that deals
390 with the size of ice crystals according to process parameters (Microwave assisted freezing Part 2:
391 impact of duty cycle and microwave energy on ice crystal size distribution).

392 Acknowledgements

393 This work received financial support from the French National Research Agency (ANR) in the
394 framework of the FREEZEWAVE project (ERANET call “SUSFOOD”, grant number ANR-14-SUSF-0001).
395 M. SADOT’s PhD work is co-funded by the FREEZEWAVE project and the Région Pays de la Loire. The
396 authors would also like to thank C. Couëdel for his technical contribution.

397 Nomenclature

398	a	Long waveguide wall length	(m)
399	b	Small waveguide wall length	(m)
400	Cp	Heat capacity	(J.kg ⁻¹ .K ⁻¹)
401	d	Product height	(m)
402	E	Electric field	(V.m ⁻¹)
403	H	Specific enthalpy	(J.kg ⁻¹)
404	h	Convection coefficient	(W.m ⁻² .K ⁻¹)
405	k	Thermal conductivity	(W.m ⁻¹ .K ⁻¹)
406	L	Product length (y axis)	(m)
407	Ls	Water latent heat of solidification	(J.kg ⁻¹)
408	l	Product width (x axis)	(m)
409	m	Mass	(kg)
410	n	Normal vector	
411	Q	Generated heat	(W.m ⁻³)
412	S	Surface (m ²)	
413	T	Temperature	(K)
414	t	Time	(s)
415	x	Mass fraction	(kg.kg _{product} ⁻¹)
416	Y	Empirical parameter of the model	(K)
417	ε ₀	Vacuum permittivity	(F.m ⁻¹)
418	ε''	Relative dielectric loss factor	
419	ρ	Density	(kg.m ⁻³)
420	ω	Pulsation	(rad.s ⁻¹)

421

422 Subscript

423	air	Air
424	alu	Aluminium
425	bw	Bound water
426	d	Defrosted/fresh
427	dm	Dry matter
428	f	Frozen
429	i	Ice
430	N2	Nitrogen
431	w	Liquid water

432 References

- 433 Anese, M., Manzocco, L., Panozzo, A., Beraldo, P., Foschia, M., & Nicoli, M. C. (2012). Effect of
434 radiofrequency assisted freezing on meat microstructure and quality. *Food Research*
435 *International*, 46(1), 50–54.
436 <http://www.sciencedirect.com/science/article/pii/S0963996911006491>
- 437 Basak, T., & Ayappa, K. G. (1997). Analysis of microwave thawing of slabs with effective heat capacity
438 method. *AIChE Journal*, 43(7), 1662–1674. <https://doi.org/10.1002/aic.690430703>
- 439 Bremer, P. J., & Ridley, S. C. (2004). Safety of Frozen Foods. In Y. H. Hui, P. Cornillon, I. Guerrero
440 Legaretta, M. H. Lim, K. D. Murrell, & W.-K. Nip (Eds.), *Handbook of Frozen Foods* (Marcel Dek,
441 pp. 595–618).
- 442 Cherbanski, R. (2011). Calculation of Critical Efficiency Factors of Microwave Energy Conversion into
443 Heat. *Chemical Engineering & Technology*, 12, 2083–2090.
444 <https://doi.org/10.1002/ceat.201100405>
- 445 Chourot, J. M., Macchi, H., Fournaison, L., & Guilpart, J. (2003). Technical and economical model for
446 the freezing cost comparison of immersion, cryomechanical and air blast freezing processes.
447 *Energy Conversion and Management*, 44(4), 559–571.
- 448 Curet, S. (2008). *Traitements micro-ondes et transferts de chaleur en milieu multiphasique*. Thèse de
449 l'Université de Nantes.
- 450 Dalvi-Isfahan, M., Hamdami, N., Xanthakis, E., & Le-Bail, A. (2017). Review on the control of ice
451 nucleation by ultrasound waves, electric and magnetic fields. *Journal of Food Engineering*, 195,
452 222–234. <https://doi.org/10.1016/j.jfoodeng.2016.10.001>
- 453 Delgado, A. E., & Sun, D.-W. (2001). Heat and mass transfer models for predicting freezing processes
454 – a review. *Journal of Food Engineering*, 47(3), 157–174.
455 <http://www.sciencedirect.com/science/article/pii/S0260877400001126>
- 456 Dempsey, P., & Bansal, P. (2012). The art of air blast freezing: Design and efficiency considerations.
457 *Applied Thermal Engineering*, 41, 71–83.
- 458 Devine, C. E., Bell, R. G., Lovatt, S., & Chrystall, B. B. (1996). Red Meat. In L. E. Jeremiah (Ed.), *Freezing*
459 *effects on food quality* (Marcel Dek, pp. 51–83).
- 460 Hafezparast-moadab, N., Hamdami, N., Dalvi-isfahan, M., & Farahnaky, A. (2018). Effects of
461 radiofrequency-assisted freezing on microstructure and quality of rainbow trout (*Oncorhynchus*

462 mykiss) fillet. *Innovative Food Science and Emerging Technologies*, 47(May 2017), 81–87.
463 <https://doi.org/10.1016/j.ifset.2017.12.012>

464 Hallstrom, B. (1990). Mass transport of water in foods - A consideration of the engineering aspects.
465 *Journal of Food Engineering*, 12(1), 45–52. [https://doi.org/10.1016/0260-8774\(90\)90018-4](https://doi.org/10.1016/0260-8774(90)90018-4)

466 Hanyu, Y., Ichikawa, M., & Matsumoto, G. (1992). An Improved Cryofixation Method - Cryoquenching
467 Of Small Tissue Blocks During Microwave Irradiation. *Journal of Microscopy-Oxford*, 165(Part 2),
468 255–271.

469 Healy, J. J., de Groot, J. J., & Kestin, J. (1976). The theory of the transient hot-wire method for
470 measuring thermal conductivity. *Physica*, 82(2), 392–408.

471 Jackson, T. H., Urgan, A., Critser, J. K., & Gao, D. (1997). Novel microwave technology for
472 cryopreservation of biomaterials by suppression of apparent ice formation. *Cryobiology*, 34(4),
473 363–372. <http://www.sciencedirect.com/science/article/pii/S0011224097920162>

474 Jha, P. K., Sadot, M., Vino, S. A., Rouaud, O., Havet, M., Le-bail, A., Jury, V., & Curet-ploquin, S. (2017).
475 A review on effect of DC voltage on crystallization process in food systems. *Innovative Food*
476 *Science and Emerging Technologies*, 42(May), 204–219.
477 <https://doi.org/10.1016/j.ifset.2017.06.002>

478 Kalichevsky, M. T., Knorr, D., & Lillford, P. J. (1995). Potential food applications of high-pressure
479 effects on ice-water transitions. *Trends in Food Science and Technology*, 6(8), 253–259.

480 Le Bail, A., Chevalier, D., Mussa, D. M., & Ghoul, M. (2002). High pressure freezing and thawing of
481 foods: a review. *International Journal of Refrigeration*, 25, 504–513.

482 Lim, M. H., McFetridge, J. E., & Liesebach, J. (2004). Frozen Food Components and Chemical
483 Reactions. In Y. H. Hui, P. Cornillon, I. Guerrero Legaretta, M. H. Lim, K. D. Murrell, & W.-K. Nip
484 (Eds.), *Handbook of Frozen Foods* (Marcel Dek, pp. 67–81).

485 Llave, Y., Mori, K., Kambayashi, D., Fukuoka, M., & Sakai, N. (2016). Dielectric properties and model
486 food application of tylose water pastes during microwave thawing and heating. *Journal of Food*
487 *Engineering*, 1–11. <http://dx.doi.org/10.1016/j.jfoodeng.2016.01.003>

488 Nelson, S. O., & Datta, A. K. (2001). Dielectric properties of food materials and electric field
489 interactions. In A. K. Datta & R. C. Anantheswaran (Eds.), *Handbook of microwave technology*
490 *for food applications* (pp. 69–114).

491 Otero, L., Ousegui, A., Guignon, B., Le Bail, A., & Sanz, P. D. (2006). Evaluation of the thermophysical

492 properties of tylose gel under pressure in the phase change domain. *Food Hydrocolloids*, 20(4),
493 449–460. <https://doi.org/10.1016/j.foodhyd.2005.04.001>

494 Pangrle, B. J., Ayappa, K. G., Sutanto, E., & Davis, H. T. (1992). Microwave Thawing of Lossy Dielectric
495 Materials. *Chemical Engineering Communications*, 112(February), 39–53.
496 <https://doi.org/10.1080/00986449208935991>

497 Rouaud, O., & Le-bail, A. (2015). *Optimizing Combined Cryogenic and Conventional*.

498 Sadot, M., Curet, S., Rouaud, O., Le-Bail, A., & Havet, M. (2017). Numerical modelling of an innovative
499 microwave assisted freezing process. *International Journal of Refrigeration*, 80, 66–76.
500 <https://doi.org/10.1016/j.ijrefrig.2017.04.017>

501 Sheen, N. I., & Woodhead, I. M. (1999). An Open-ended Coaxial Probe for Broad-band Permittivity
502 Measurement of Agricultural Products. *Journal of Agricultural Engineering Research*, 74, 193–
503 202.

504 Singh, R. P., & Heldman, D. (2014). Food Freezing. *Introduction of Food Engineering*, 540.
505 <https://doi.org/10.1016/B978-0-12-398530-9.00007-3>

506 Taoukis, P., Davis, E. A., Davis, H. T., Gordon, J., & Talmon, Y. (1987). Mathematical Modeling of
507 Microwave Thawing Modified Isotherm Migration Method. *Journal of Food Science*, 52(2).

508 Wang, W., Zhao, C., Sun, J., Wang, X., Zhao, X., Mao, Y., Li, X., & Song, Z. (2015). Quantitative
509 measurement of energy utilization efficiency and study of influence factors in typical
510 microwave heating process. *Energy*, 87, 678–685. <https://doi.org/10.1016/j.energy.2015.05.036>

511 Woo, M., & Mujumdar, A. (2010). Effects of Electric and Magnetic Field on Freezing and Possible
512 Relevance in Freeze Drying. *Drying Technology*, 28(4), 433–443.
513 <http://www.tandfonline.com/doi/abs/10.1080/07373930903202077>

514 Xanthakis, E., Le-Bail, A., & Ramaswamy, H. (2014). Development of an innovative microwave
515 assisted food freezing process. *Innovative Food Science and Emerging Technologies*, 26, 176–
516 181. <http://dx.doi.org/10.1016/j.ifset.2014.04.003>

517 Zhang, H., & Datta, A. K. (2005). Heating concentrations of microwaves in spherical and cylindrical
518 foods. Part two: in a cavity. *IChemE*, 83(March), 14–24. <https://doi.org/10.1205/fbp.04047>

519

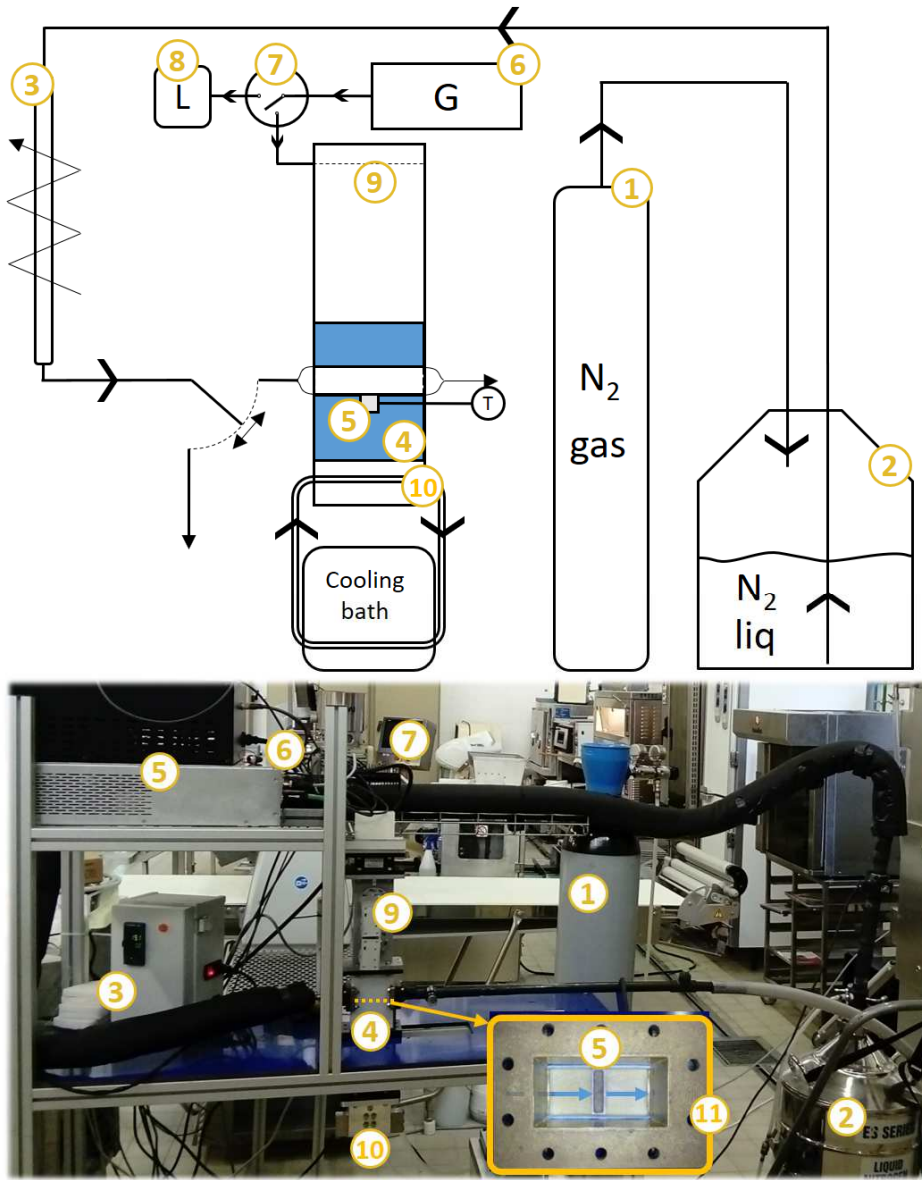
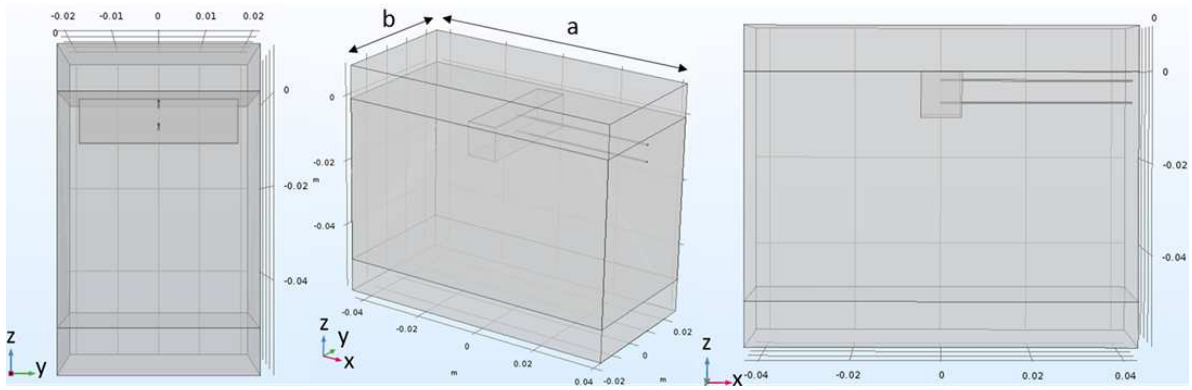


Figure 1: Scheme and photography of the experimental device of microwave assisted freezing process.

a)



b)

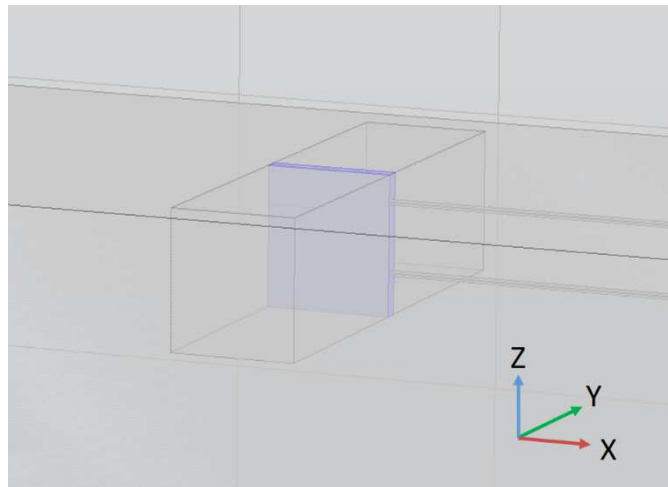


Figure 2: a) Geometry used to perform microwave assisted freezing trials and simulations, with thermocouples locations; b) layer on which the heat equation was solved for the hybrid model.

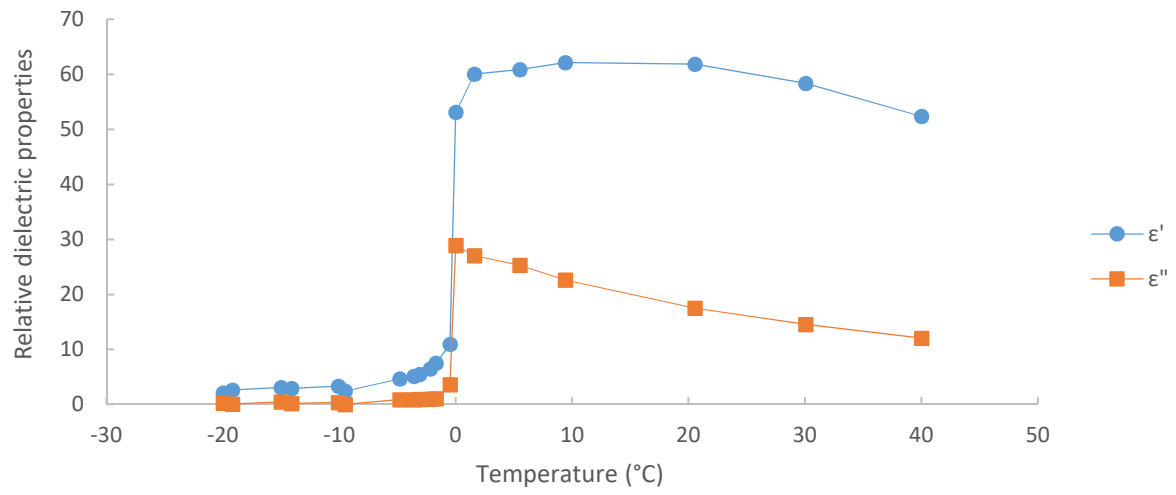


Figure 3: Dielectric constant (ϵ') and dielectric loss factor (ϵ'') as a function of temperature.

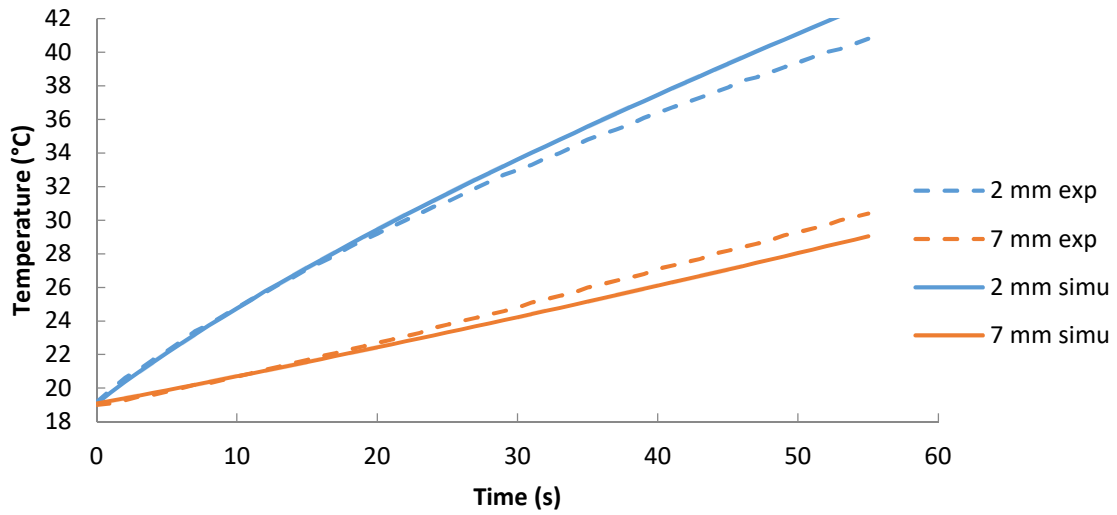


Figure 4: Comparison between experimental and simulated temperatures at 2 mm and 7 mm deep for a microwave heating at a measured power of 10.9 W (generator) with a resulting power of 8.2 W after using the calibration factor.

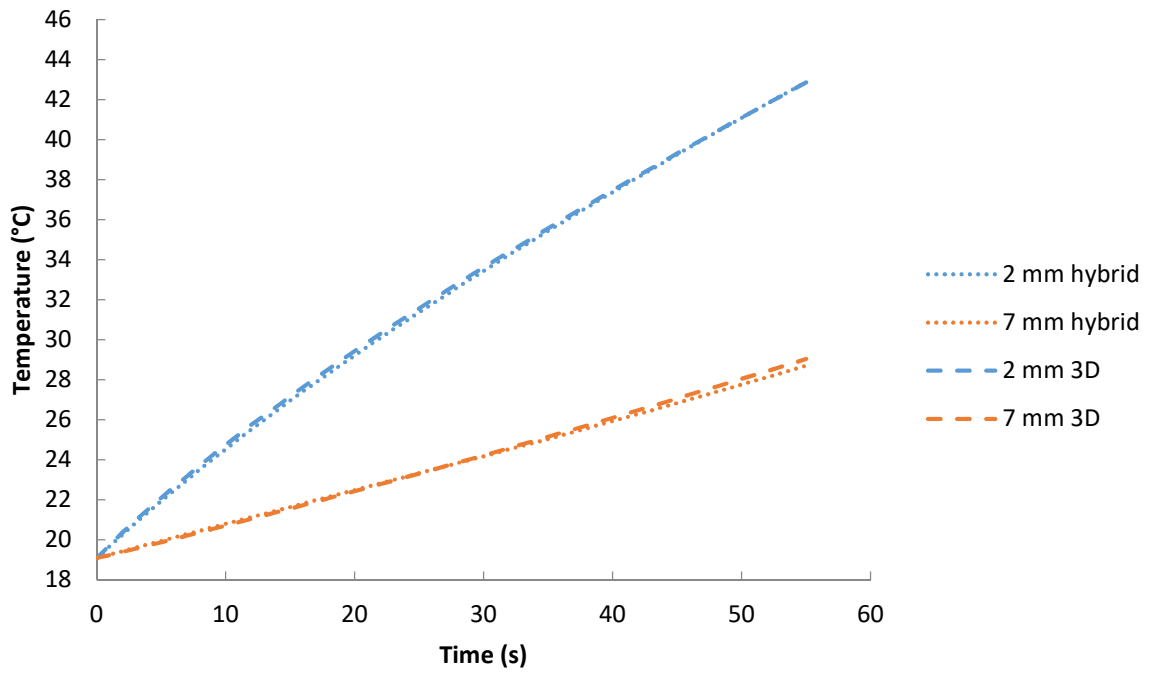


Figure 5: Comparison between hybrid and 3D model for a microwave heating.

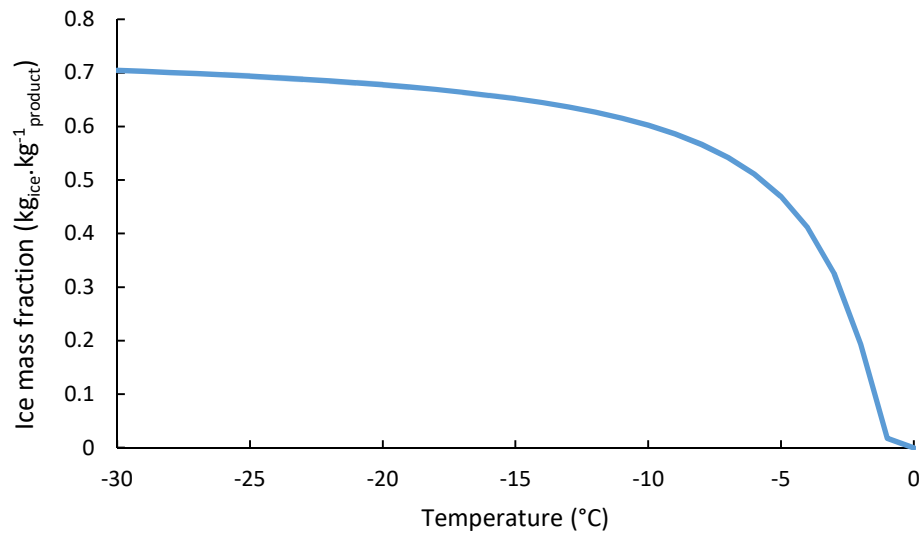
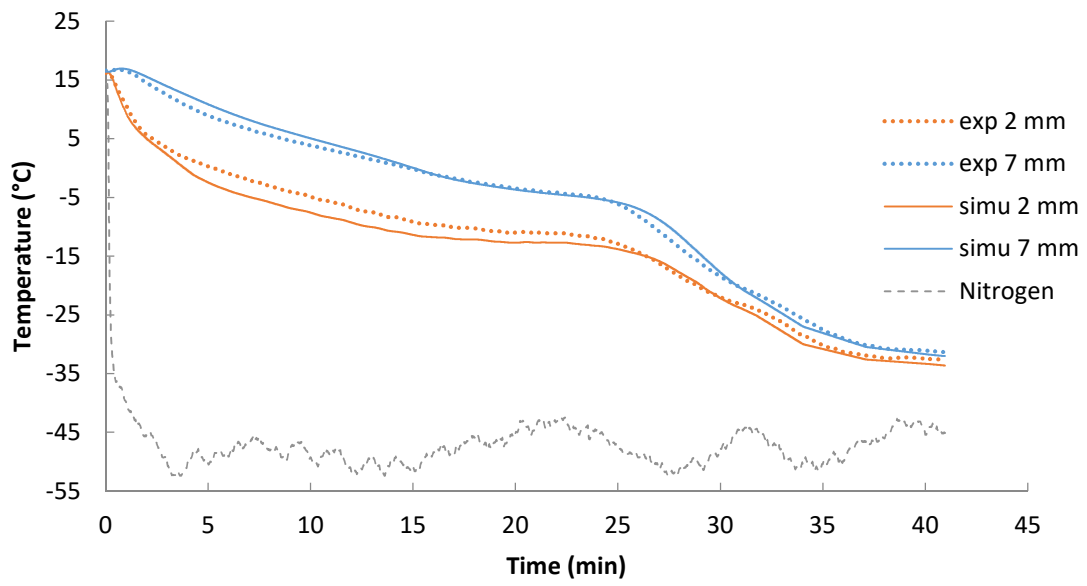


Figure 6: Ice mass fraction as a function of temperature for an empirical parameter Y set to 0.75 K

a)



b)

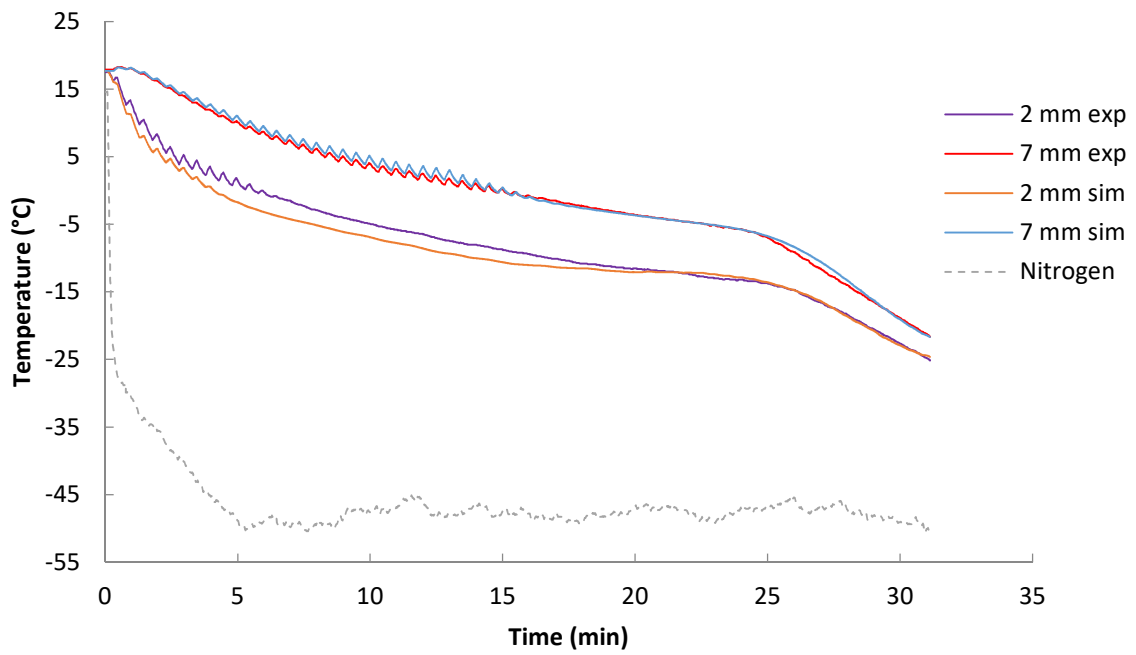


Figure 7: Comparison of temperature curves of a microwave assisted freezing a) for continuous application at a power of 1W; b) for a duty ratio of 0.33, a period of 30 s, at a power of 3 W.

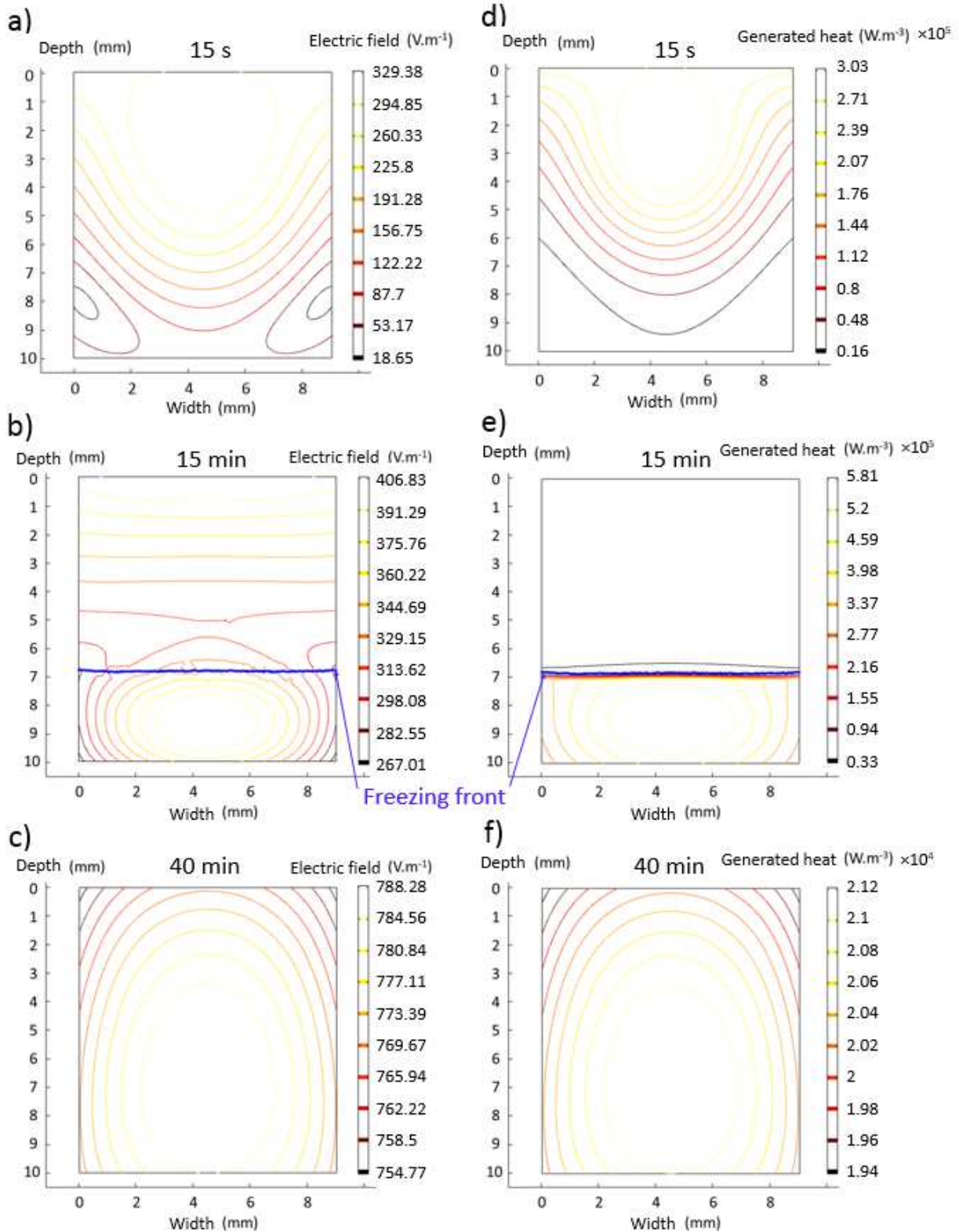


Figure 8: Electric field distribution in a) fresh state; b) during freezing; c) in frozen state; and generated heat in d) fresh state; e) during freezing; f) frozen state, on the x - z product central section ($y = 0$).

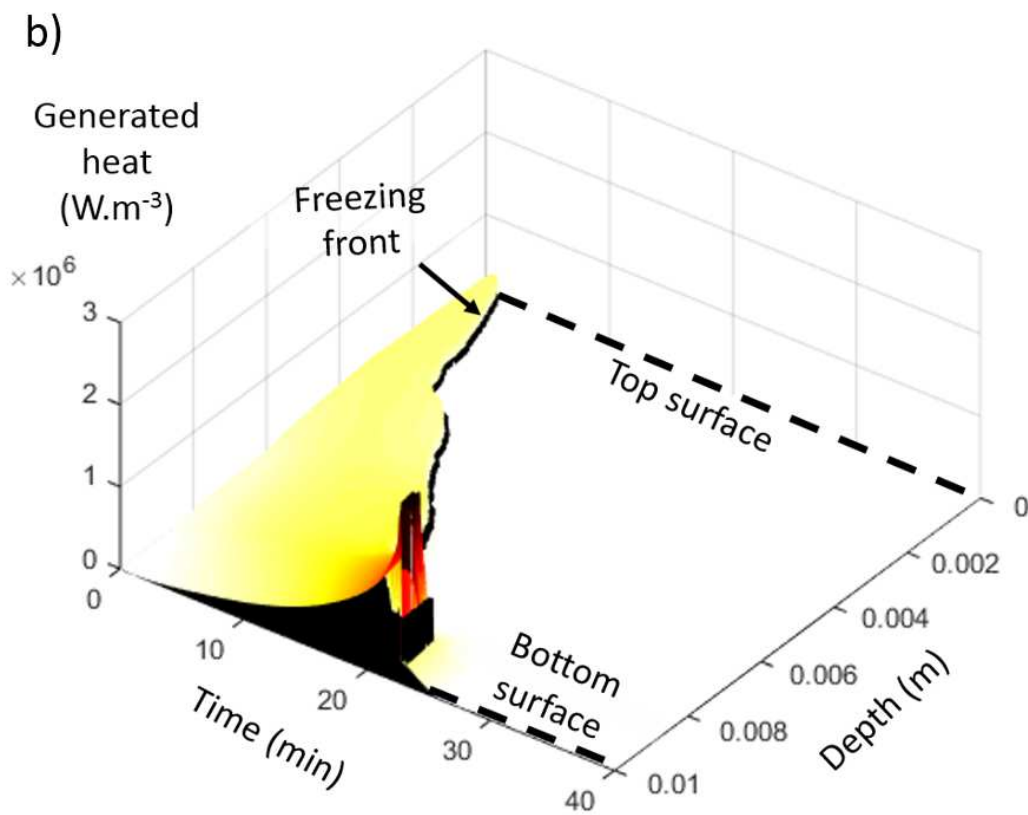
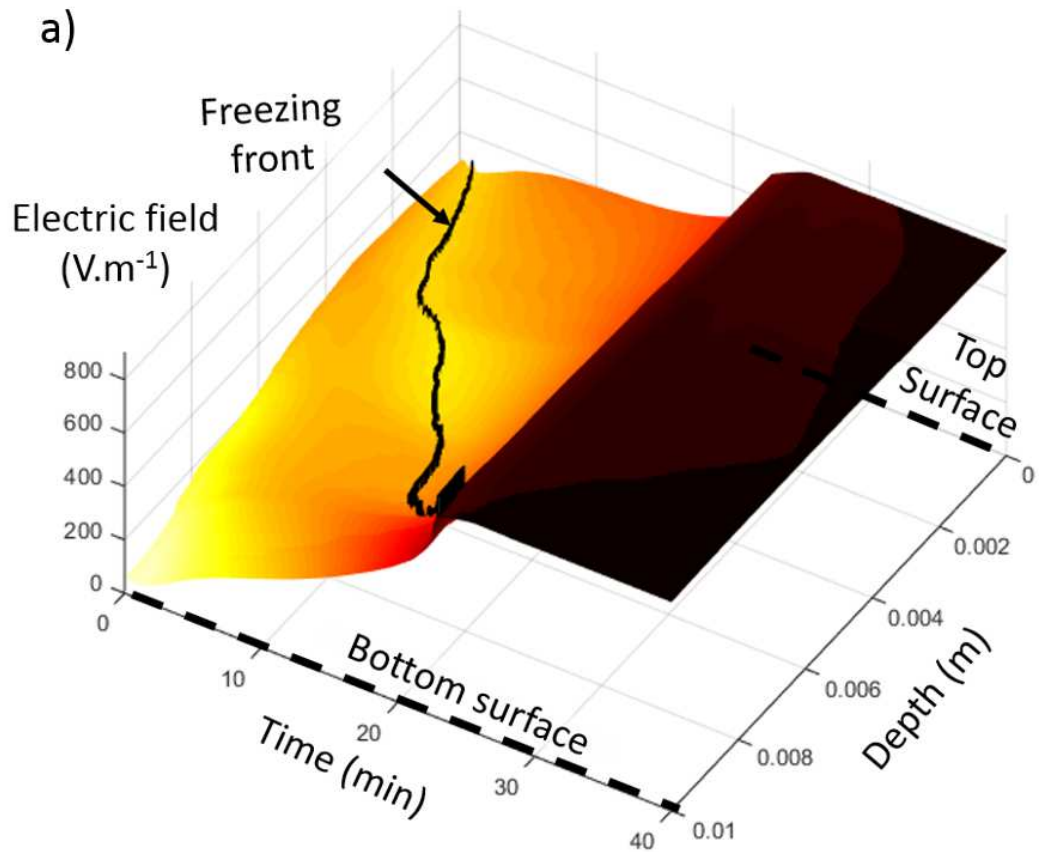


Figure 9: a) Electric field distribution; b) Generated heat distribution on the product z central axis ($x = 0$; $y = 0$) as a function of time and depth.

Table 1: Methylcellulose gel thermal conductivity at several temperatures, measured by hot-wire probe method.

Temperature (°C)	-25	-20	-15	5
Thermal conductivity (W.m⁻¹.K⁻¹)	1.670 ± 0.031	1.595 ± 0.279	1.556 ± 0.035	0.533 ± 0.018

Table 2: Latent heats measured by DSC during freezing and thawing of methylcellulose gel.

	Peak integration (kJ.kg ⁻¹)	
	Freezing	Thawing
Trial 1	250.54	254.05
Trial 2	251.74	256.59
Mean latent heat (kJ.kg⁻¹)	253.23	

Table 3: Methylcellulose gel heat capacity in fresh and frozen phase.

		Trial 1	Trial 2	Mean
Heat capacity	Fresh (20°C)	3924.20	3881.18	3902.69
(J.kg⁻¹.K⁻¹)	Frozen (-20°C)	2626.44	2587.8	2606.91

1 *Table 4: Convection coefficient between nitrogen and aluminium bloc.*

	Trial 1	Trial 2	Trial 3	Trial 4	Trial 5	Trial 6	Trial 7	Mean	Standard deviation
Convection coefficient (W.m⁻².K⁻¹)	124.5	118.0	125.1	86.2	123.5	104.2	109.5	113.0	14.3

2